THE JOURNAL OF PHYSICAL CHEMISTRY C

Article

pubs.acs.org/JPCC

Catalytic Role of Minority Species and Minority Sites for Electrochemical Hydrogen Evolution on Metals: Surface Charging, Coverage, and Tafel Kinetics

Ya-Hui Fang, Guang-Feng Wei, and Zhi-Pan Liu*

Shanghai Key Laboratory of Molecular Catalysis and Innovative Materials, Department of Chemistry, Key Laboratory of Computational Physical Science (Ministry of Education), Fudan University, Shanghai 200433, China

Supporting Information

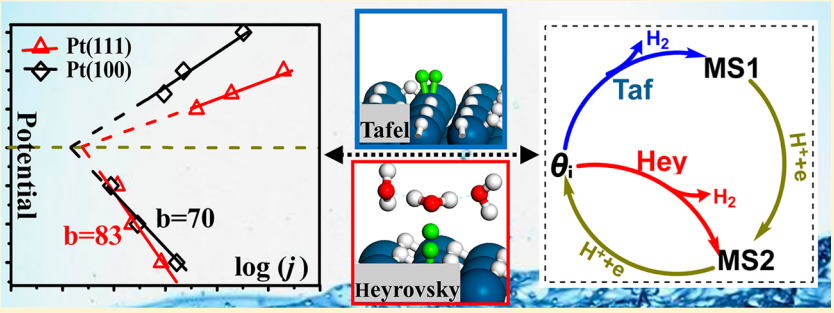

ABSTRACT: Hydrogen evolution reaction (HER: $H^+ + e^- \rightarrow {}^1/_2H_2$) on metals exhibits the characteristic kinetics of electrocatalytic process. Here a theoretical method based on the constant-charge first principles periodic continuum solvation model is proposed to resolve the potential-dependent reaction kinetics on Pt and Au surfaces, and the quantitative linkage is established between the Tafel kinetics (current vs potential) and the electrochemical condition, including the surface structure, the surface charging, and the coverage. The theoretical Tafel slopes for HER are determined to be 83 mV on Pt(111) and 70 mV on Pt(100), which are generally associated with the reactions involving the *minority weakly adsorbed H*, i.e. the atop H above 1 ML on Pt(111) and the bridging H above 1.5 ML on Pt(100). The mechanism and the contribution of each pathway (Volmer, Tafel, and Heyrovsky pathways) are determined quantitatively. It is revealed that HER at the minority surface steps has a much higher activity than at terraces, which is responsible for the overall activity on a typical Pt electrode. The theoretical model here paved the way toward the large-scale computational screening for both active and economic hydrogen electrode.

1. INTRODUCTION

Electrocatalytic HER was regarded as the prototypical reaction in electrochemistry, based on which the Tafel equation is derived experimentally in 1900s by Swiss chemist Julius Tafel. As hydrogen is a critical energy carrier in the renewable energy cycle, HER has received considerable attention in recent years. Although Pt was known to be the most efficient electrocatalyst that can convert proton and electrons to H_2 near the equilibrium potential (0 V vs SHE), the prohibitive cost of Pt has limited severely the large-scale applications. Continued research efforts have been devoted to develop new strategies that can replace Pt (via non-Pt materials) or reduce Pt usage (e.g., dispersing into nano- or subnanoparticles) while maintaining the high activity.[1−7] This has led to the renewed interest on the reaction kinetics at the atomic level aiming to answer the fundamental questions, (i) why Pt is indispensable and (ii) where is the active site for Pt.

While the early experimental studies suggested that HER is not structure sensitive to the surface crystallography,[8,9] the modern research tends to favor the conclusion that the activity depends on the surface structure and thus the size of the nanoparticle. By conducting voltammograms measurement on single-crystal surfaces at different conditions, the Markovic[10−12] and Conway groups[13,14] have shown that the activity of HER and its reverse, hydrogen oxidation reaction (HOR) varies on different exposed surfaces. The Markovic group showed that reaction activity of HOR/HER increases with the sequence (111) < (100) < (110) at acid and alkaline solution: the exchange current density is 0.45, 0.60, and 0.98 mA/cm^2 for (111), (100), and (110) in 0.05 M H_2SO_4 at 303 K,[11] whereas Conway reported that HER activity order is (100) < (111) < (110) under acid and alkaline conditions.[13,14] The reported activity order for (100) and (111) surfaces is different, and Conway suggested that this could be due to the specific experimental conditions, including pH, surface coverage, and the electrolyte anions.[15] Nevertheless, the ridged (110) surface is always more active (ca. two times) than the two terraces. In accordance with this, the Hoshi group found that the exchange current density (j_0) increases linearly with the increase of the step density and they concluded that the stepped sites are the

Received: January 18, 2013
Revised: March 7, 2013
Published: March 25, 2013

   dx.doi.org/10.1021/jp400608p | J. Phys. Chem. C 2013, 117, 7669−7680

active site of HER/HOR.[16−18] Since smaller nanoparticles contain more surface defects/steps, it is inferred that the activity should increase upon the decrease of the particle size and the increase of activity by 2−5 times upon the decrease of the Pt particle size from 2 to 6 nm was indeed reported.[19,20] Babic et al., however, showed that the specific activity of HOR is similar for Pt nanoparticles with the mean particle size of 2.5−3.5 nm.[21] Apparently, the observed variation of the HER/HOR activity on differently structured Pt is not dramatic (e.g., within 1 order of magnitude). This is intriguing as two opposite explanations are both plausible, i.e. (i) HER occurs only at a small number of defects/stepped sites and the activity scales with the concentration of such defects, and (ii) HER is truly structure insensitive and can occur on all surface sites with the similar activation barrier, where the activity scales with the exposed surface area.

The kinetics of HER/HOR on metal surfaces is not straightforward due to the electrochemical condition: multiple pathways and multiple surface phases could be coexisting, which are strongly influenced by the electrochemical potential. The nature of the rate-determining step of HER/HOR on Pt remains elusive and a microscopic model on the potential-dependent kinetics is not established yet. Specifically, it is still being debated whether H_2 formation proceeds via the direct Tafel coupling ($2H^* \leftrightarrow H_2$) between two adsorbed H (H^*), or the proton-coupled bond forming via the Heyrovsky reaction ($H^* + H^+ + e^- \leftrightarrow H_2$), or both. This is also reflected from the scattered experimental data on the Tafel slop for HOR: on (111) the slope ranges from 30 to 74 mV and on (100) it is from 30 to 112 mV[9,11] (in electrochemistry, the slope of the Tafel curve is often utilized as an indication of the mechanism according to the Butler−Volmer equation[22]). Wang et al.[23] suggested that HOR on Pt electrodes might proceed via dual pathways, including both Tafel and Heyrovsky mechanisms. Using microkinetics modeling, they found that a Tafel−Volmer mechanism at a low H coverage (<0.3 ML) can produce the best fit with the experiment rate around the equilibrium potential. The low H coverage is, however, not supported by experiment[24] and first-principles calculations.[25,26]

To elucidate the puzzle, theoretical simulations mainly based on density functional theory (DFT) calculations have been utilized to probe the atomic level detail of the reaction.[27−34] For example, the Norskov group found that HER on both Pt(111) and Pt(100) surfaces prefer the Tafel pathway using a static water bilayer model. The calculated barriers on the two surfaces are similar, ∼0.85 eV at the equilibrium potential.[25] Because of the difficulties in describing the complex electrochemical conditions including the surface charging, the solid−liquid interface, and the potential in the standard DFT packages, a direct comparison between theory and experiment on the Tafel kinetics of HER is not available to date.

It is a central task of this work to establish a systematic method for evaluating the kinetics of the multistep electrocatalytic process as represented by HER. Here we utilize the recently developed first-principles periodic continuum solvation model (DFT/CM-MPB)[35−37] to deduce the Tafel kinetics of HER/HOR on typical Pt and Au surfaces, namely, Pt(111), Pt(100), and Au(111) under acidic conditions (pH 0), and correlate the kinetics with the surface charging, the coverage, and the potential. The current DFT/CM-MPB method allows the consideration of concurrent effects due to the solid surface, the water solution, and the electrochemical potential at the reaction conditions in one unified theoretical framework. The low-energy-reaction pathways at the concerned potentials are identified and the potential-dependent kinetics are resolved from theory. By comparing the HER activity between theory and experiment on different surfaces and metals, we propose a general model to optimize HER catalyst via computation and present a practical strategy for designing new catalysts.

2. METHODS

All DFT calculations were performed by using the SIESTA package with numerical atomic orbital basis sets[38,39] and Troullier−Martins normconserving pseudopotentials.[40] The exchange-correlation functional utilized was at the generalized gradient approximation level, known as GGA-PBE.[41] The optimized double-ζ plus (DZP) polarization basis set was employed. All transition states (TSs) of the catalytic reaction were searched by using our recently developed methods within the Constrained-Broyden Scheme.[42−44] For the (111) and (100) surfaces, we utilized $p(3 \times 2\sqrt{3})$ (12 atoms per layer) and $p(4 \times 4)$ (16 atoms per layer) six-layer slabs with adsorbates on both sides of the surfaces, respectively. The other calculation details are the same as those described in our previous work.[45,46] The accuracy of the calculated energetics was examined by benchmarking the results from SIESTA with those from the plane-wave methodology and the difference in adsorption energy is generally below 0.05 eV for H (e.g. the H differential free energy of adsorption (with respect to the free energy of the gas-phase H_2 at the standard state) at 1 ML on Pt(100) is calculated to be 0.29 eV from SIESTA and 0.26 eV from the plane-wave method).

The solid/liquid interface was described by using the periodic continuum solvation model based on the modified Poisson−Boltzmann equation (CM-MPB), which can take into account the long-range electrostatic interaction due to the solvation of electrolyte.[35,46,47] The DFT/CM-MPB method has been utilized to calculate the electro- and photo-catalytic reactions at the solid−liquid interfaces,[35,36,47] and compute the fundamental properties of metal surfaces in solution, such as the potential of zero charge and the differential capacitance, where the calculated values show good agreement with the available experimental data.[46] Within the DFT/CM-MPB model, we describe the solvated proton at the solid−liquid interface using the solvated $H_3O^+(H_2O)_2$ complex where the first solvation shell of H_3O^+ is included explicitly and the rest of the solution is represented by the CM-MPB model. In this model, two of the Hs of H_3O^+ are hydrogen bonded with the nearby water molecules and the remaining H interacts with the surface to initiate the HER process.

It should be noted that as for the other electronic structure calculation methods, the DFT/CM-MPB method is performed on the basis of the constant-charge framework, in which a surface slab at a fixed net charge (q) can be routinely calculated. As there are two surfaces per slab, the surface net charge Q_{net} equals half of the total net charge q, $Q_{net} = q/2$. The neutralizing charge ($-q$) is distributed in the vacuum region of the slab following the modified Poisson−Boltzmann equation, mimicking the polarized ionic charge distribution (diffuse layer) in solution.[35] The constant-charge model in calculation is, however, not exactly what is used in experiment, where the electrode is held under a certain potential. We therefore need to convert the kinetics data collected at certain charge q to that at a certain potential U, which can be summarized briefly as follows (for more detail see section 3.2).

For an elementary reaction, the free energy barrier $\Delta G_a(q=0,\theta_i)$ at the potential of zero charge ($q = 0$) condition can be obtained first by using eq 1,

$$\Delta G_a(q, \theta_i) = G_{TS}(q, \theta_i) - G_{IS}(q, \theta_i) \quad (1)$$

$$\Delta G_a(U, \theta_i) = \Delta G_a(q, \theta_i)|_{q \Leftrightarrow U} \quad (2)$$

where θ_i indicates the surface phase characterized by a particular local coverage i and $G_{TS/IS}$ are the free energies at the TS/IS (IS: initial state). This step involves the location of the relevant TS and ISs at the charge neutral condition, as is typical in standard periodic DFT packages. Next, one needs to establish the linkage between the charge q and the potential U. This is done by carrying out a series of calculations with a variable q and simultaneously measuring the potential U of each q state by using DFT/CM-MPB. The absolute electrochemical potential of the system (a surface slab) can be measured by computing the work function in solution and then referring it to the experimental work function of the standard hydrogen electrode (SHE, 4.4−4.8 V from experiment and 4.6 V utilized in this work). In this way, the free energy barrier at a certain U can be obtained as eq 2. The free energy correction (referring to the standard state) to the DFT/CM-MPB total energy can be derived by using the standard thermodynamics equations (see, for example, ref 48).

3. RESULTS

The Volmer (Vol) step is the initiating step for HER, which is followed by the H−H bond-formation steps, either the Heyrovsky step (Hey) or the Tafel step (Taf), as illustrated in Scheme 1. Under reaction conditions, there could be a number of possible coexisting phases, as indicated by the local H coverage θ_i. Knowing the exact surface phase is kinetically important because the reaction barrier is sensitive to the local bonding environment, including the number and the geometry of the preadsorbed H atoms. In the following, we first utilize the thermodynamics analyses (section 3.1) to identify the most likely coverages at the concern potentials. The reaction channels on all the likely phases will then be calculated in section 3.2, based on which the overall rate and its potential dependence can be deduced.

Scheme 1. Reaction Pathways and Surface Coverages for HER[a]

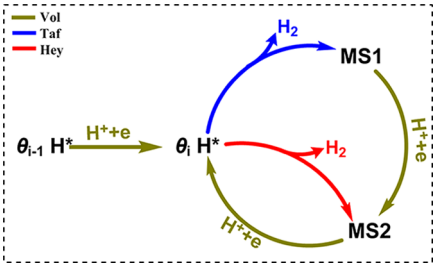

[a]The elementary steps include the Volmer (Vol), the Tafel pathway (Taf), and the Heyrovsky (Hey) steps. MS1: the state with two H* removed. MS2: the state with one H* removed.

3.1. H-Covered Surface Phases. In the grand canonical ensemble, the H on the surface can be considered to be in equilibrium with the solvated proton in solution. This requires that the Volmer step, the charging/discharging of solution H_3O^+ to H*, is sufficiently fast compared to the other reactions, e.g. those to break/form the H−H bond. With this assumption (the validity of the assumption will be addressed later), we can utilize the following procedure to calculate the H coverage at different potentials.

First, the reaction free energy $\Delta G_{\theta i}(U)$ of $H^+ + e^- \leftrightarrow H^*|_{\theta_i}$ is calculated at different phases θ_i and different potentials, U. The previous work has shown that because the potential affects much more strongly the energy of proton and electron compared to the adsorption state of H*,[49] a simple thermodynamics approach based on neutral slab calculations is accurate enough to calculate $\Delta G_{\theta_i}(U)$. At each phase, the charged-slab calculations using DFT/CM-MPB have been utilized to determine the potential of zero charge ($PZCl_{\theta_i}$) and correlate the exact surface net charge Q^i_{net} with the potential.

Second, the relative portion of a phase at U, $x_i(U)$, is obtained by using eq 3 from Boltzmann distribution. The overall H coverage at the potential U ($\theta(U)$) and the overall surface net charge ($Q_{net}(U)$) can finally be derived by summing the contribution from all phases by using eq 4.

$$x_i(U) = \frac{e^{-\Delta G_{\theta_i}(U)}}{\sum_i e^{-\Delta G_{\theta_i}(U)}} \quad (3)$$

$$\theta(U) = \sum_i (\theta_i \times x_i(U)); \quad Q_{net}(U) = \sum_i (Q^i_{net} \times x_i(U)) \quad (4)$$

Following the above procedure, we have determined $\theta(U)$ and $Q_{net}(U)$ on Pt(111), Pt(100), and Au(111) surfaces. The results are plotted in Figure 1 and the important data at 0 V are collected in Table 1. In general, we found that on all the surfaces the H coverage is highly dependent on the applied electrochemical potential. By decreasing the electrochemical potential, one can gradually build up the surface H. At the same potential, the H coverage on Pt(100) surface is the highest and that on Au(111) is the lowest among the three surfaces.

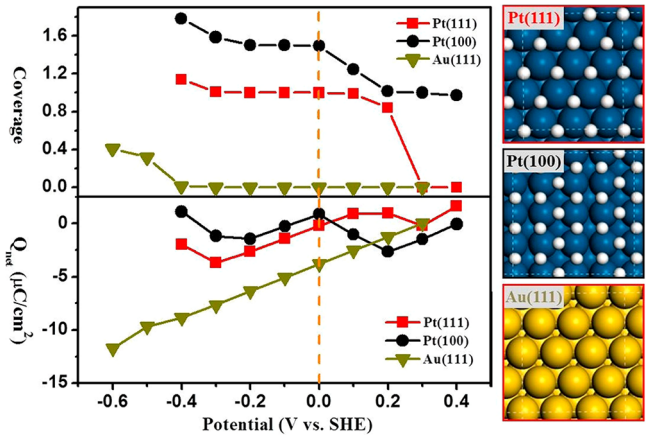

Figure 1. The diagrams of the coverage vs potential and the surface net charge (Q_{net}) vs potential for Pt(111), Pt(100), and Au(111). The dominant surface phases at 0 V for Pt(111) (1 ML H coverage), Pt(100) (1.5 ML H coverage), and Au(111) (0 ML H coverage) are also shown on the right panels.

Unlike the behavior of the coverage, the surface net charge is oscillating around zero on Pt surfaces but increases steadily on

dx.doi.org/10.1021/jp400608p | J. Phys. Chem. C 2013, 117, 7669−7680

Table 1. The Surface Properties at 0 V for Pt(111), Pt(100), and Au(111) (Only the Representative Surface Phases Are Listed)

phase θ_i	x_i(0 V)	$\Delta G_{\theta i}$(0 V) (eV)	$PZC\|_{\theta_i}$ (V)	CN[a]	$d_{H\text{-}M}$ (Å)[b]
0.92 ML/ Pt(111)	0.003	−0.19	0.08	3	1.84/1.84/1.92
1 ML/ Pt(111)	0.997	−0.15	0.02	3	1.87/1.85/1.88
1.08 ML/ Pt(111)	1.05×10^{-6}	0.35	−0.10	1	1.56
1.44 ML/ Pt(100)	0.074	−0.05	−0.01	2	1.73/1.73
1.5 ML/ Pt(100)	0.913	−0.06	−0.08	2	1.74/1.74
1.56 ML/ Pt(100)	7.19×10^{-6}	0.30	−0.17	2	1.72/1.76
0.08 ML/ Au(111)	2.14×10^{-8}	0.48	0.27	3	1.90/1.94/1.95

[a]CN is the coordination number of the least stable H* at θ_i. [b]$d_{H\text{-}M}$ is the bond distance between the least stable H* and the surface metal atom.

Au(111) with the decrease of potential (Figure 1, bottom panel). This is because the H coverage increases continuously on Pt surfaces, which consumes the accumulated surface negative charges; on Au(111), on the other hand, the surface is free of H atom at the potentials above −0.4 V and the decrease of potential leads to the accumulation of negative charges on the surface. Obviously, the surface net charge on all the phases at the concerned potential is generally within 10 $\mu C/cm^2$, which corresponds to ∼0.04 lel per surface metal atom. Although these values are rather small (e.g., 5%) compared to the typical overall charge measured for the desorption of the adsorbed H layer, 200−300 $\mu C/cm^2$ on Pt surfaces[10,22,50] (mainly due to the discharging of H to proton), we will show later that the kinetics of some surface reactions (e.g., Heyrovsky reaction) is very sensitive to the surface charging and thus the knowledge on the exact surface net charge is critical for determining kinetics.

On Pt(111), the H coverage around 0 V is about 1 ML. This corresponds to the structural configuration that all surface fcc hollow sites are occupied by one H* (see Figure 1, right panel), which agrees with previous DFT studies (using the adsorption energy of H without other corrections[51,52]). Below −0.3 V, the coverage increases further with the atop sites being occupied by H* appreciably. At 0 V, the concentration of the atop H* is low [(8.7×10^{-6})%] and the surface is dominated by the 3-fold H*. Consistently, the H coverage on Pt(111) is measured to be larger than $\sim^2/_3$ ML near 0 V using voltammetries.[24,53] The 3-fold hollow site H* is referred to the underpotential deposited (UPD) hydrogen in experiment and it emerges below 0.35 V vs SHE.[15] The atop H* that is referred to the overpotential deposited (OPD) hydrogen has also been identified by ATR-FTIRAS utilizing the SEIRAS technique,[54,55] the signal of which becomes evident below 0 V.

On Pt(100), the H coverage is about 1.5 ML at 0 V and the coverage is larger than 1.5 ML below −0.2 V. The 1.5 ML H coverage corresponds to the configuration that all H atoms sit at the bridge sites and each Pt is coordinated with three H atoms (see Figure 1, insert). Both experiment and previous theoretical calculations have suggested that the H coverage should be above 1 ML on Pt(100) at the equilibrium potential[24,26] (at 1 ML each surface Pt atom is bonded with two bridging H atoms). From our results, we can assign the extra 0.5 ML bridging H above 1 ML to be the OPD H on Pt(100) referred in experiment.[56] Obviously, there is no atop H* on Pt(100) at the potential concerned.

On Au(111), the surface is essentially free of H atoms at 0 V and only below −0.4 V does the H coverage start to build up slowly. At the low coverage limit (e.g., 0.083 ML), our DFT/CM-MPB calculation shows that the H adsorption free energy on Au(111) is +0.48 eV (with respect to the gas phase H_2), while it is −0.34 eV on Pt(111). This is consistent with the general consensus that Au has a much weaker covalent bonding ability compared to Pt.

It should be mentioned that the determination of the exact coverage with use of thermodynamics alone could be problematic as the kinetics may be vital. For example, it may well be likely that the charging/discharging of H_3O^+ to adsorbed H is so slow that the H thermodynamic equilibrium coverage could not be reached at the operating temperature. The coverage presented in Figure 1 is thus only the up-limit coverage. Nevertheless, Figure 1 provides a useful guide on the surface coverage condition for studying kinetics. We will show in the following that the thermodynamics equilibrium assumption holds nicely on Pt, a good catalyst for HER, but breaks down on Au, a poor catalytic material.

3.2. Reaction Mechanism. In the following, we focus on HER/HOR kinetics close to the equilibrium potential (0 V). As the mechanism and the kinetics are potential dependent, we will mainly illustrate the mechanism at 0 V. We started from Pt(111) to gather a general view of the HER process via the two different pathways, Tafel and Heyrovsky, as shown in Scheme 1; we then examined the Pt(100) surface to verify whether the special structure and a different H coverage will modify the activity. Finally, to further shed light on the activity variation across different metal surfaces, we compared the Pt surfaces with the less active Au(111) surface.

We found that the Volmer step (S-Figure 1, Supporting Information) occurs with a low barrier on Pt surfaces (<0.2 eV) at the concerned potentials, but is highly activated on Au(111). Because of this, the Volmer step is not presented in the pathways on Pt surfaces for clarity, and it is included in the pathways on Au(111).

3.2.1. Pt(111). For Pt(111) at ∼0 V, the thermodynamics analyses tells that the H coverage is around 1 ML. We therefore calculate Tafel and Heyrovsky pathways on 0.92, 1.0, 1.08 ML H/Pt(111) phases, in total six different pathways. The representative free energy profile for HER on 1.0 ML H/Pt(111) at 0 V via the two pathways is shown in Figure 2 and the data are listed in Table 2. Our procedure to calculate the free energy profile at the potential U is outlined in the following.

First, we need to calculate the free energy profile at the zero charge (q = 0) condition for all the pathways that could occur on different phases. To this end, the key states along the pathway, including the IS, TS, and final state (FS), are determined and thus the free energy barriers ($\Delta G_a(\theta_i,q=0)$) are obtained (see eq 1). It is noted that at the q = 0 condition, the electrochemical potential ($PZC|_{\theta_i}$) of different phases is not exactly 0 V. As listed in Table 1, $PZC|_{\theta_i}$ for the 0.92, 1.0, 1.08 ML H/Pt(111) is 0.08, 0.02, −0.10 V vs SHE, respectively. The obtained $\Delta G_a(\theta_i,q=0)$ for Pt(111) is listed in S-Table 1, Supporting Information.

dx.doi.org/10.1021/jp400608p | J. Phys. Chem. C 2013, 117, 7669−7680

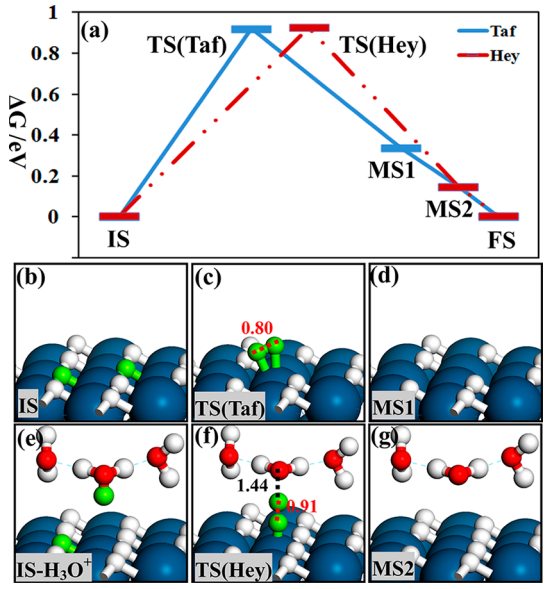

Figure 2. (a) The free energy profile via Tafel and Heyrovsky pathways on 1 ML H/Pt(111) at 0 V. M The meaning of the states (MS1, MS2) is the same as those in Scheme 1. The located IS, TS, MS1, and MS2 for the Tafel step (b–d) and the Heyrovsky step (e–g) are also shown. The labeled distances are in angstroms. The produced H_2 molecule is omitted at the FS for clarity. Large ball: Pt atoms. Small red ball: O atoms. Small white/green ball: H atoms.

Table 2. Calculated Free Energies of Elementary Steps for HER on 1 ML H/Pt(111) at 0 V[a]

elementary steps	ΔE	$\Delta H(0\rightarrow 298K)$	ΔZPE	$-T\Delta S$	ΔG
		Tafel			
Sur → TS	0.94	0	−0.02	0	0.92
Sur → MS1 + H_2	0.69	0.09	−0.03	−0.41	0.34
MS1 + H^+ + e → MS2	−0.37	−0.04	0.02	0.21	−0.19
MS2 + H^+ + e → Sur	−0.32	−0.04	0.02	0.21	−0.15
		Heyrovsky			
Sur → TS	0.91	0	−0.14	0.15	0.92
Sur + H^+ + e → MS2 + H_2	0.32	0.04	−0.02	−0.21	0.15
MS2 + H^+ + e → Sur	−0.32	−0.04	0.02	0.21	−0.15

[a]The $\Delta H(0\rightarrow 298K)$ is deduced from the standard thermodynamic data.[57]

Second, we calculate the free energy profiles at 0 V for all the pathways. By using the DFT/CM-MPB method, it is possible to calculate ΔG_a of the reactions at 0 V, $\Delta G_a(\theta_i 0\ V)$, by tuning (adding or extracting) the number of electrons on the surface using eq 2. At this stage, the calculated $\Delta G_a(\theta_i 0\ V)$ of each pathway is referred to the phase (θ_i) where it occurs. The obtained $\Delta G_a(\theta_i 0\ V)$ for Pt(111) are listed in S-Table 2, Supporting Information.

$$\Delta G_a(U) = \ln[\sum_i x_i(U) e^{\Delta G_a(\theta_i, U)}] \quad (5)$$

Third, we derive $\Delta G_a(0\ V)$ of the Tafel and the Heyrovsky pathway at 0 V by using eq 5 (see the Supporting Information for the derivation of eq 5). This step is to correct the energy difference between different phases (as reflected in the $x_i(U)$ term) and sum up the contributions from different phases. For Pt(111) at 0 V, the 1 ML H phase is dominant and the 0.92 and 1.08 ML phases have only a minor contribution (see Table 1). $\Delta G_a(0\ V)$ on Pt(111) are thus calculated to be 0.92, 0.92 eV for the Tafel and Heyrovsky pathway, respectively, which are essentially the same as those on 1 ML H/Pt(111), ΔG_a(1 ML,0 V). At the lower potentials, the major contributing phase is switched to the higher coverage phases and will be discussed later.

As shown above, a major challenge in computing the activity of an electrochemical reaction from first principles arises from the separation of the surface charging effect and the electrochemical potential effect. Because the current CM-MPB method is on the basis of the constant charge DFT framework, a one-to-one mapping between the charge and the potential needs to be established. Since a number of possible H covered phases are present at a potential, this mapping has to be done for many possible phases. The accuracy for predicting the electrochemical potential of surface is therefore critical to the kinetics of the electrocatalytic process at the solid/liquid interface. The calculated PZC for a series of metal surfaces and the differential capacitance on Pt using the DFT/CM-MPB method have been benchmarked carefully with the experimental and a good agreement has been found.[46] This is due to the fact that the DFT/CM-MPB method can correctly take into account the solvation effect and the long-range electrostatic screening of electrolyte.

For Pt(111) at 0 V, the two pathways have the same overall free energy barrier. In the Tafel pathway, the two H* couple to form the H_2 molecule. At the TS, the two reacting Hs sit on the top site of Pt with the H–H distance being 0.80 Å (Figure 2c). In the Heyrovsky pathway, the reaction occurs via an adsorbed H* reacting with a solvated proton in the presence of a surface electron. At the TS, the proton passes its H to the atop H, yielding a H--H--OH_2 complex with the H--OH_2 distance being 1.44 Å (Figure 2f). It is noticed that the TS in both pathways involves the activation of the adsorbed H atom from its initial fcc hollow site to the atop site.

Although the Tafel and the Heyrovsky pathway have the same ΔG_a at 0 V, the variation of ΔG_a with respect to the potential is expected to be different since there is one electron involved in the Heyrovsky reaction but no explicit electron transfer is required in the Tafel reaction. To quantify the potential dependence of the kinetics, we have calculated ΔG_a of the two elementary reactions on 1 ML H/Pt(111) at different potentials using the charged-slab DFT/CM-MPB method and the results are plotted in Figure 3.

We found that the calculated ΔG_a of the Heyrovsky reaction decreases linearly with the increase of the potential U, while ΔG_a of the Tafel reaction is rather constant over the

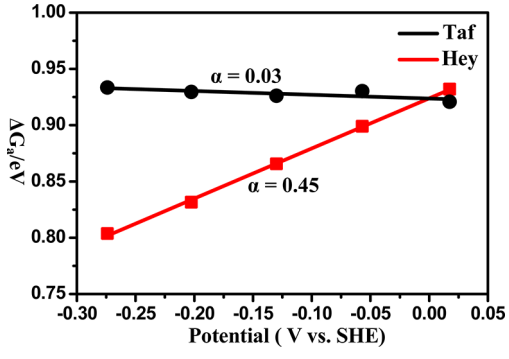

Figure 3. The potential dependence of the reaction barrier (ΔG_a) for the elementary Tafel and Heyrovsky reaction on 1 ML H/Pt(111).

dx.doi.org/10.1021/jp400608p | J. Phys. Chem. C 2013, 117, 7669–7680

investigated potentials. By fitting linearly the barrier∼overpotential relation ($\Delta G_a = \Delta G_a^0 - \alpha F\eta$; $\eta = U$), we can deduce that the charge transfer coefficient α is 0.46 and 0.03 for the Heyrovsky and Tafel reactions, respectively. These determined α values confirm the general assumption in electrochemistry that α is ∼0.5 for an ideal single electron transfer elementary reaction and 0 for the nonelectron transfer reaction.

3.2.2. Pt(100). Similarly, we have investigated HER on Pt(100). At 0 V the H coverage for Pt(100) is 1.5 ML from thermodynamics and therefore the investigations on kinetics were conducted on four coverages around 1.5 ML, namely 1.38, 1.44, 1.5, and 1.56 ML. ΔG_a(0 V) on Pt(100) are calculated to be 0.91, 1.10 eV for the Tafel and Heyrovsky pathways, respectively, which are mainly due to the reactions on the 1.5 ML phase (the other three phases have only minor contribution to the overall activity at 0 V). The representative free energy profile of the two pathways on 1.5 ML H/Pt(100) at 0 V is thus shown in Figure 4. The complete kinetics data are listed in S-Tables 3 and 4, Supporting Information.

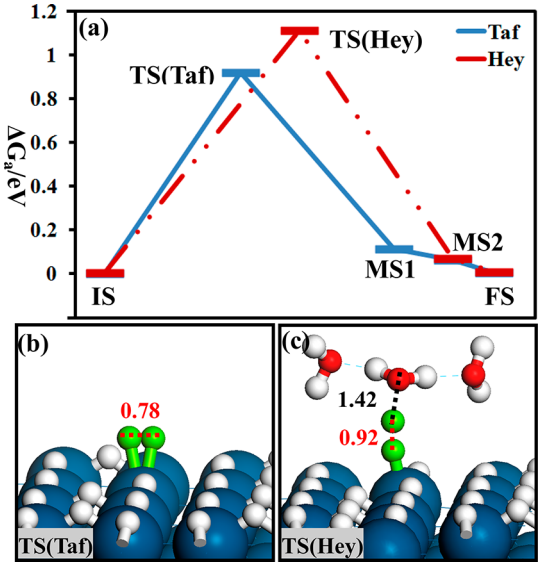

Figure 4. (a) The free energy profile on 1.5 ML H/Pt(100) at 0 V. The meaning of the states (MS1, MS2) is the same as those in Scheme 1. (b and c) TSs of the Tafel and Heyrovsky pathways.

From Figure 4, we can see that the Tafel pathway is the lowest energy pathway and the calculated ΔG_a is nearly identical to that on Pt(111). The Heyrovsky pathway on Pt(100) has a barrier of 1.11 eV, being obviously higher than the Tafel pathway. These indicate that (i) Pt(100) is not more active than Pt(111), although the equilibrium H coverage on the surface is much higher, and (ii) only one major reaction mechanism, i.e., the Tafel pathway, is present on Pt(100) around 0 V, being different from the scenario on Pt(111).

In the Tafel pathway, two H* atoms initially at the bridge site couple to generate H_2. At the TS, both H atoms are activated to the atop site on the same Pt atom with the H−H distance being 0.78 Å (see Figure 3b). The nearest adsorbed H* to the TS complex is only 2.31 Å, indicating an obvious bonding competition exists between the TS complex and the coadsorbed H atoms. For the Heyrovsky pathway, the TS is also similar to its counterpart on Pt(111), as shown in Figure 3c, with one H_3O^+ in solution reacting with an atop H*.

From the results on Pt(111) and Pt(100), we can summarize that (i) the atop [H−H] complex for TS is common for HER on Pt surfaces and (ii) the H−H distance at the TS is around 0.8−1.0 Å (cf. 0.73 Å for the gas phase H_2), and the surface coupling reaction (Tafel mechanism) generally has a shorter H−H distance at the TS compared to that in the Heyrovsky mechanism.

It is of interest to compare our calculated energetics with those reported previously, although the theoretical methods (DFT/CM-MPB) utilized in this work differ from the previous work. Apparently, the reported barrier for the HER/HOR reaction from previous DFT calculations varies significantly, from ∼0.1 to ∼0.85 eV.[25,31,52] This is because, as also demonstrated in this work, both the surface coverage and the solvation effect are critical to the HER/HOR kinetics. Nevertheless, at the representative surface coverage, namely, 1 ML H/Pt(111), the barrier of HER/HOR calculated was generally high, e.g. above 0.7 eV. For example, the Norskov group suggested that the rate-determining step of HER is the Tafel reaction and the barrier is ∼0.85 eV.[25] Santos et al. has also calculated activation energy for dissociation hydrogen at various coverages. They found that the barrier is about 0.73 eV at 1 ML[52] (the barrier of the same reaction from this work is 0.92 eV by including the solvation effect.

3.2.3. Au(111). To provide a deeper insight into the reaction kinetics of HER, we also investigated HER on the less active Au surface, which should help us to outline the critical factors to HER kinetics. At 0 V, the Au(111) surface is largely free of adsorbed H atoms from thermodynamics due to the low adsorption energy of H atoms on Au. From Scheme 1, no H_2 can be generated directly on the clean Au(111) phase; by elevating the H coverage via the Volmer step, the Tafel and the Heyrovsky reactions can then take place. It should be pointed out that the Volmer step on Au is highly activated and has been included in the reaction mechanism to address the overall activity.

We have investigated the Tafel and Heyrovsky pathways on 0.16 and 0.08 ML H/Au(111) phases. The free energy profile is shown in Figure 5. We found that (i) the Volmer step has a high reaction barrier of 0.95 eV, which corresponds to the

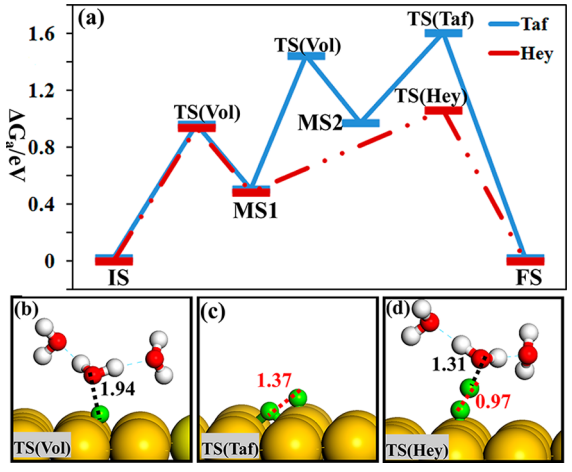

Figure 5. The free energy profile for HER on Au(111) at 0 V. MS1 and MS2 correspond to the clean surface with one and two additional H*, respectively. (b, c, and d) The located TSs of the Volmer reaction and H−H bond formation in the Tafel and Heyrovsky pathways, respectively.

dx.doi.org/10.1021/jp400608p | J. Phys. Chem. C 2013, 117, 7669−7680

Table 3. The Calculated Potential-Dependent Tafel Currents and Heyrovsky Currents of the Three Surfaces

	Pt(111)		Pt(100)		Au(111)	
U (V)	$\log(j_{Taf/Hey})$	$\log(j_{tot})$	$\log(j_{Taf/Hey})$	$\log(j_{tot})$	$\log(j_{Taf/Hey})$	$\log(j_{tot})$
0		−6.6[a]		−6.8[a]		−10.4[a]
−0.05	−6.1/-6.5	−5.9	−6.1/−9.0	−6.1	−17.4/−9.4	−9.4
−0.10	−5.8/-6.1	−5.6	−5.5/−8.6	−5.5	−15.7/−8.5	−8.5
−0.15	−5.3/-5.5	−5.1	−4.8/−8.3	−4.8	−14.0/−7.2	−7.2
−0.2	−4.5/-4.5	−4.2	−4.0/−8.2	−4.0	−12.3/−6.8	−6.8

[a]$\log(j_{tot})$ extrapolated to 0 V, that is $\log(j_0)$.

reduction of one proton to form a fcc H* on the bare Au(111). In line with the calculated high barrier, the located TS for the Volmer step is FS like, with a long dissociating H--OH_2 distance, 1.94 Å. (ii) Once the H* is present, the elementary reaction to form the H−H bond is in fact not so difficult at 0 V. For example, the barrier of the Tafel (elementary) reaction is only 0.63 eV. However, due to the low stability of the H*, the overall ΔG_a for the two pathways is very high on Au(111), being 1.06 and 1.59 eV at 0 V, which is at least 0.14 eV higher than that of the lowest energy pathway on Pt(111). The Volmer−Heyrovsky mechanism is clearly favored compared to the Volmer−Tafel mechanism.

It is of interest to further compare the structure of TS on the Au surface with those on Pt surfaces. For the TS of the Heyrovsky reaction on Au(111), the dissociating H--OH_2 distance is 1.31 Å, being ∼0.1 Å shorter than that on Pt surfaces, and the forming H--H distance is 0.97 Å, being ∼0.05 Å longer than that on Pt surfaces. These indicate that the TS is more IS like on Au(111), which agrees with the facts that the IS of the reaction (H* on Au(111)) is unstable and the TS is more close to IS. For the TS of the Tafel reaction, the TS structure is achieved with the H−H bond being 1.37 Å, which is again longer than those identified on Pt surfaces, indicating the TS is also IS like for the Tafel reaction. At the TS, one H atom absorbs at the atop site and the other one sits at the bridge site (Figure 5c).

3.3. Tafel Plot. With all the potential-dependent kinetics data available, we are now at the position to deduce the HER/HOR kinetics according to microkinetics. The overall current j_{tot} is a function of potential U, which can be calculated by summing up the contribution, j_p, from all the pathways (labeled by subscript p) at the potential U, as written in eq 6. For a particular reaction pathway, the current, j_p, is expressed as the net current of the oxidation (j_O) and reduction (j_R) currents, and j_O or j_R can be calculated by using the standard rate equation, as eq 8, in which A is the preexponential factor (it is set as 10^{13} at 300 K); S is the total surface area; [site] is the concentration of the reactive site (ML); and $\Delta G_a(U)$ is calculated from eq 5.

$$j_{tot} = |\sum_p j_p| \tag{6}$$

$$j_p = j_O - j_R \tag{7}$$

$$j_{O/R} = AFS^{-1}N_A^{-1}e^{-\Delta G_a(U)/RT}[\text{site}] \tag{8}$$

In electrochemistry, it is often more convenient to combine the rate equation (eq 8) with $\Delta G_a = \Delta G_a(U_0) - \alpha F\eta$ to link the Tafel slope with the charge transfer coefficient α, i.e. $b = RT/\alpha F$. For α being 0.5, the Tafel slope will be 120 mV, which corresponds to the rate-determining step being an elementary one-electron transfer reaction (half an electron is transferred at the TS). By measuring the Tafel slope, it is therefore straightforward to deduce how many electrons transferred before the rate-determining step.

Using eqs 1−8, we have calculated potential-dependent Tafel and Heyrovsky currents of the three surfaces and the data for HER at the negative potentials are listed in Table 3. By extrapolating j_{tot} to the equilibrium potential, j_0, we found that j_0 for the two Pt surfaces is $\sim 10^{-7}$ A cm^{-2}, which is, not surprisingly, 3 orders of magnitude larger than that on Au(111).

For Pt(111), as shown in Table 3, j_{tot} comprises the contribution from both Tafel and Heyrovsky pathway at the low overpotentials (0 to −0.2 V). In contrast, for Pt(100), j_{tot} is mainly from the Tafel mechanism and the Heyrovsky mechanism is negligible to the overall current. On Au(111), the Heyrovsky mechanism prevails.

We then plotted j_{tot} vs U for the two Pt surfaces in Figure 6, where the apparent Tafel slope (b) can be estimated according to $b = \partial\eta/\partial\log(j_{tot})$. The theoretical calculated slope for Pt(111) is 30 and 83 mV at the positive and the negative potentials, respectively, while those for Pt(100) are 50 and 70 mV. These apparent Tafel slopes are generally small, being in the range of 45−90 mV (α: 1.5−0.75) for HER, and 30−60 mV (α: 2−1) for HOR.

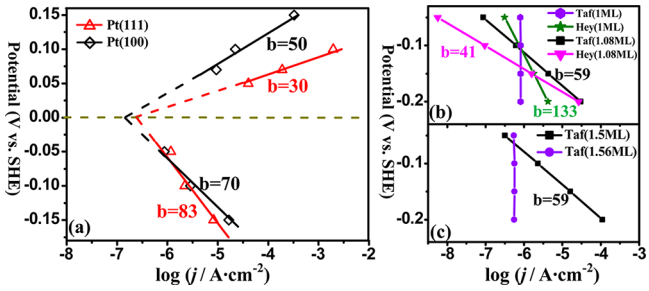

Figure 6. (a) Tafel plot (U vs $\log(j)$) for HER on Pt(111) and Pt(100). (b) Tafel plots of the Tafel and Heyrovsky pathways on 1 and 1.083 ML H/Pt(111). (c) Tafel plots for Tafel pathways on 1.5 and 1.56 ML H/Pt(100).

From the theoretical Tafel plot, it is clear that on Pt surfaces j_{tot} is not solely determined by one pathway on one single surface phase. Because multiple reaction channels and multiple surface phases are present, the apparent Tafel slope is influenced by all the potential-dependent factors, such as the barrier of the elementary reactions and the surface coverage. To reveal the origin of the apparent Tafel slope, we therefore decompose j_{tot} into the contributions from each pathway on each phase and plot the major contributing current against the potential, as shown in parts b and c of Figure 6 for Pt(111) and Pt(100). We found that not only the elementary reaction

dx.doi.org/10.1021/jp400608p | J. Phys. Chem. C 2013, 117, 7669−7680

barrier but also the surface coverage have important effects on j_{tot} and on the apparent Tafel slope.

For Pt(111), as shown in Figure 6b, both the Tafel and Heyrovsky pathways and both 1 and 1.083 ML H/Pt(111) surface phases are kinetically important at the HER condition. This agrees with the previous suggestion that HER may follow dual pathways on Pt(111).[11,23] It is obvious that the Heyrovsky and Tafel pathways on 1.083 ML H/Pt(111) are critical to determine the overall apparent Tafel slope (83 mV). This is interesting because the major contributing phase to HER current is the 1 ML H/Pt(111) at 0 V (see section 3.1) but it turns out to be the 1.083 ML H/Pt(111) below −0.1 V. The additional atop H* (from 1 to 1.083 ML) thus plays an important catalytic role in HER on Pt(111). The number of electrons transferred in producing the atop H* (the Volmer step) that occurs before the rate-determining H−H bond formation steps enters finally into the rate equation, yielding the overall Tafel slope of 83 mV.

For Pt(100), the coverage-dependent kinetics is quite similar to that on Pt(111), although the H coverage and the surface structure are different. As shown, the major contributing phase at 0 V (i.e., 1.5 ML) is in fact not the main contributor to the overall current at the negative potentials just below −0.06 V. It is the Tafel pathway (b = 59) at 1.56 ML H/Pt(100) that determines largely the overall Tafel slope (b = 70). From these theoretical results, we can conclude that the minority surface phases with additional unstable H* species are in fact the weakly adsorbed phases that are responsible to HER current.

It might be mentioned that the prediction of the pH effect on the HER/HOR kinetics is also likely under the current theoretical framework. In S-Figure 2, Supporting Information, we have investigated the HER activity change by lifting pH 0 to pH 2. We found that (i) the pH increase will shift the equilibrium potential down to −0.118 V (−0.059 V per PH unit), which is due to the thermodynamics. (ii) The HER current at the same overpotential decreases by less than one time (132%) when the pH is lifted (log(j) is −5.92 for pH 0 and −6.04 for pH 2 at 0.05 V overpotential, respectively). This is mainly due to the diminished contribution from the Heyrovsky pathway when the proton concentration in solution drops. In experiment, Markovic reported that j_0 is about 2−20 times larger in the acid condition (pH 1) than that in the alkaline condition (pH 13)

4. GENERAL DISCUSSIONS ON HER ACTIVITY

By combining extensive DFT/CM-MPB calculations with thermodynamics and microkinetics, we show that the HER activity follows the order Pt(111) ≈ Pt(100) > Au(111). The mechanism of HER varies on different surfaces. On Pt(111) it follows a mixed mechanism with both Tafel and Heyrovsky pathways; on Pt(100) it is dominated by the Tafel mechanism; and on Au(111) it always follows the Volmer−Heyrovsky mechanism.

4.1. Pt vs Au. Since both Tafel and Heyrovsky mechanisms are permitted for H−H bond formation on Pt and Au, this implies that the exact pattern for H−H bond formation is not the key factor for making a good HER catalyst. We can understand this phenomenon as follows. Because the H atom generally prefers to be at the top site to react (the top site is, however, not the site H atom initially adsorbs), the best way to form the H−H bond needs to be to reduce maximally the lateral repulsion between the reacting complex (at the atop site) and the preadsorbed H atoms (at the nearby hollow or bridge sites). For the surface with a densely packed H layer, such as that in Pt(100) (1.5 ML H), the Tafel mechanism is preferred, in which two surface H* couple at the sites they initially stay; on the other hand, on the surface phase with a less densely packed H layer, such as Pt(111) and Au(111), the reaction channel of the Heyrovsky mechanism opens.

In fact, Pt distinguishes from Au in the Volmer step. The Volmer step is facile on Pt but is highly activated on Au. Our results show that whether the Volmer step is facile on the metals is not much related to thermodynamics, but is controlled by kinetics. For example, the newly arrived atop H* onto the 1 ML H/Pt(111) is unstable (+0.35 eV) at 0 V and the barrier of the Volmer step is still not high (<+0.4 eV) with the TS being close to the FS. In contrast, on the bare Au(111), while the additional H (fcc H*) is similarly unstable (+0.48 eV) at 0 V, the Volmer step is highly activated with a barrier of 0.95 eV.

$$E_{1s} = \frac{\int_{-\infty}^{E_F} \rho\varepsilon \, d\varepsilon}{\int_{-\infty}^{E_F} \rho \, d\varepsilon} \tag{9}$$

To understand the electronic structure of the reacting H in the Volmer step, we have plotted the projected density of states (pDOS) onto the 1s orbital of the reacting H atom on Pt(111) and Au(111) at 0 V at the IS and the TS (Figure 7). At the ISs,

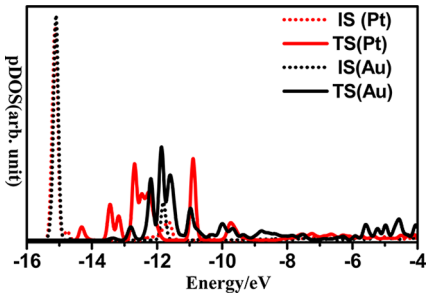

Figure 7. Projected density of states (pDOSs) onto 1s of the reacting H at IS and the TS of the Volmer step on Pt(111) and Au(111) at 0 V vs SHE.

the major bonding peak of the H (i.e., in the solvated H_3O^+) locates at ∼15 eV for both Pt and Au. At the TSs, the pDOS peaks of the H shift up in energy, apparently due to the interaction of the H atom with the surface states (including the metal d states). The major bonding peak of the H atom on Au(111) at the TS locates at −12 eV but the antibonding peaks also appear below the Fermi level (−4.6 eV, i.e. 0 V vs SHE). On Pt(111), the bonding peaks of the H spans from −15 to −10 eV and no antibonding peaks can be identified below the Fermi level. By utilizing eq 9, we can measure the energy of H_{1s} states, E_{1s}, which reveals that E_{1s} is −11.6 eV on Pt, and −10.3 eV on Au. This indicates that the TS can be better stabilized on Pt, where the H−Pt antibonding orbitals are not occupied.

The lower barrier of the Volmer step on Pt could therefore be understood as follows. The low stability of the H on 1 ML H/Pt(111) is mainly due to the lateral repulsion and the surface-mediated bonding competition with the other pre-adsorbed H atoms.[58] This repulsion can be effectively reduced at the TS, where the surface Pt atom interacting with the coming H is lifted up and the other preadsorbed H atoms relax away from the coming H (see the Supporting Information for the TS of the Volmer reaction on Pt). In contrast, the low

dx.doi.org/10.1021/jp400608p | J. Phys. Chem. C 2013, 117, 7669−7680

stability of H on Au(111) is intrinsic due to the fact that the antibonding states between the H 1s orbital and the fully occupied d states of Au are partially occupied. This picture also holds at the TS where the coming H atom cannot be much stabilized through the interaction of its 1s orbital with the Au d states.[59]

4.2. The Active Site. We are now finally at the position to discuss why Pt is unique as HER catalyst. We show that Pt(111) has a very similar HER activity as Pt(100) (see Figure 6), but the calculated exchange current density (j_0) is generally lower than that measured in experiment for Pt catalyst.[11,16] But, why? A plausible explanation is that the surface sites other than (111) and (100) terraces could be more active. This therefore asks for a general but simple model for predicting the HER activity on metals without recourse to exhaustive computation on all reaction pathways on all the possible phases.

From our analyses on the Tafel kinetics, we find that the dominant HER current originates from the surface phase, where the additional unstable H* are present. On Pt(111), such additional H* is the atop H* that is present just above 1 ML, and on Pt(100), this corresponds to the extra bridging H* that appears above 1.5 ML. A generalized reaction profile as shown in Figure 8 could therefore be utilized to understand HER activity on a catalyst. To initiate HER, at least one additional H* is required on the surface, the adsorption free energy (ΔG_{H^*}) of which can be either positive or negative (with respect to the H^+/e^- at 0 V). Obviously, both too positive and too negative ΔG_{H^*} will lead to a high overall ΔG_a.[60,61] It is expected that ΔG_{H^*} should be close to zero in order to minimize the overall ΔG_a. This is the thermodynamics prerequisite for a good HER catalyst. Indeed, on Pt(111) and Pt(100), ΔG_{H^*} is similar and generally not far away from zero when HER occurs. ΔG_{H^*} of the additional H* is +0.35 eV at 1.083 ML H/Pt(111) and +0.30 eV on 1.56 ML H/Pt(100). Unfortunately, by using ΔG_{H^*} alone, it is hard to predict the activity difference between Pt(100) and Pt(111).

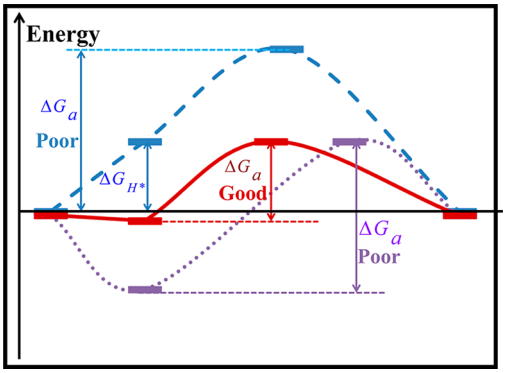

Figure 8. A generalized free energy profile for HER on electrode at 0 V. For a good HER catalyst, ΔG_{H^*} of the active H* should be close to zero in order to minimize the overall ΔG_a.

To search for a good HER catalyst, we can first utilize ΔG_{H^*} as a thermodynamics quantity to screen the potentially active phase on a catalyst, the value of which should be as close as possible to zero. Next, we need to locate the TS of a Tafel or a Heyrovsky reaction on the phase to finally predict the activity. The second step takes into account the kinetics information and thus any subtle change in the local electronic and geometrical structure would be reflected in the change of the overall barrier. By using this approach, it is obvious that Au(111) can be ruled out as a good catalyst even at the first stage because ΔG_{H^*} on Au(111) is never close to zero, being at least +0.48 eV. On Pt(111), ΔG_{H^*} is close to zero at 1 ML (−0.15 eV), while on Pt(100) ΔG_{H^*} is also close to zero at 1.5 ML (−0.06 eV).

Using this approach, we have investigated the monatomic Pt steps as represented by the stepped Pt(211) (a monatomic step linking (111) and (100) terraces) in order to identify the active site of HER on Pt. We found that ΔG_{H^*} on 1 and 1.11 ML Pt(211) is close to zero, being −0.06 eV and −0.01 eV, suggesting that these surface phases are qualified as a good HER catalyst thermodynamically. Next, we searched for the TS of the Tafel reaction on the 1 and 1.11 ML H/Pt(211) (the TS structures are shown in S-Figure 3, Supporting Information). At the TS on 1.11 ML H/Pt(211), an atop H* at the step edge reacts with another terrace H*. Interestingly, we found that the calculated ΔG_a are 0.86 and 0.55 eV at 0 V on the two surface phases. Since the 1.11 ML coverage on Pt(211) emerges close to 0 V with its ΔG_{H^*} being −0.01 eV, it is indicated that at 0 V, the HER barrier on Pt(211) is only around 0.55 eV. On the other hand, the proportion of 1.083 ML coverage on Pt(111) is less than 10^{-6} according to Boltzmann distribution (because the atop H at the 1.083 ML has a poor ΔG_{H^*}, being +0.35 eV) and the dominant phase at 0 V is 1 ML on Pt(111) with the HER barrier being close to 0.92 eV.

According to microkinetics and the above data for Pt(211) and Pt(111), even if we assume Pt polycrystalline catalysts only contain around 0.1% the concentration of the active sites, such as the monatomic steps, the overall current, estimated to be $\sim 10^{-4}$ A/cm^{-2} (a typical value observed in experiment[11,16]), is still contributed majorly from these active sites. Indeed, the previous experiment shows that the HER activity increases rather linearly with the increase of the step density.[17] We expect that HER on Pt is in fact extremely structure sensitive and the reaction occurs dominantly on the minority monatomic steps instead of the majority terrace sites. Considering the observed high H coverage (>1 ML) and the ambient reaction conditions, these stepped sites may well be reconstructed from terrace sites in situ during the electrocatalytic reaction and the dynamic structure change leads to the apparent weak dependence of HER/HOR current on the surface structure and particle size.[21,62] The surface reconstruction or, more severely, the corrosion at the high H coverage should therefore be considered explicitly in order to judge the activity of any potential HER metal catalyst. Our ongoing work has found that Pd metal, although it has the similar activation barrier of HER as Pt, can undergo significant H-corrosion at the reaction condition and thus cannot be a stable HER catalyst.

5. CONCLUSION

This work represents a comprehensive theoretical survey of HER kinetics on metals, as represented by Pt and Au surfaces. At the HER condition, there are a range of possible surface phases and on each phase there are two possible reaction channels, i.e. Tafel pathway and Heyrovsky pathway. By using the DFT method integrated with a periodic continuum solvation model based on modified-Poisson−Boltzmann electrostatics, a theoretical framework to map out the potential-dependent kinetics is proposed, through which the calculated data from the constant-charge model are converted to those at the constant potential condition. The free energy profiles of all the pathways are calculated on Pt(111), Pt(100),

dx.doi.org/10.1021/jp400608p | J. Phys. Chem. C 2013, 117, 7669−7680

and Au(111), and the potential-dependent reaction kinetics are then deduced. The main results are outlined as follows.

(i) With use of thermodynamics, the surface H coverage and the surface net charge at different potentials are determined on all surfaces. The dominant local H coverage on Pt(111), Pt(100), and Au(111) is 1, 1.5, and 0 ML, respectively, at 0 V vs SHE. The surface net charge is generally below 10 $\mu C/cm^2$ at the reaction conditions.

(ii) The HER activity follows the order Pt(111) ≈ Pt(100) > Au(111). The Volmer step is generally facile compared to the H−H bond formation step on the Pt surfaces, but is highly activated on Au. The mechanism of HER varies on different surfaces. On Pt(111) it follows a mixed mechanism with both Tafel and Heyrovsky pathways, on Pt(100) it is dominated by the Tafel mechanism, and the Volmer−Heyrovsky mechanism prevails on Au(111).

(iii) The theoretical Tafel slopes for HER are determined to be 83 mV on Pt(111) and 70 mV on Pt(100), which are generally associated with the reactions involving a small amount of weakly adsorbed H, i.e. atop H above 1 ML on Pt(111) and bridging H above 1.5 ML on Pt(100).

By quantifying the contribution from each individual pathway to the overall current and comparing the activity on Pt and on Au, we suggest that both thermodynamics and kinetics criterions need to be included for designing a good HER catalyst. Thermodynamically, the adsorption free energy of weakly adsorbed H should be about zero; and kinetically, the TS of the H−H bond formation, either in the Tafel or the Heyrovksy mechanism, should be maximally stabilized. Using this rule, we show that HER on Pt is highly structural sensitive, in which the minority monatomic steps dominate the overall activity on a typical Pt electrode. The theoretical model presented in this work shows that the large-scale computational screening for both active and economic hydrogen electrode is now within reach.

■ ASSOCIATED CONTENT

Supporting Information

Illustration (S-Tables 1−4) of the stepwise conversion of the reaction free energy (ΔG_a) of HER on Pt(111) and Pt(100) on different phases at the constant charge condition to those at the constant potential (e.g., 0 V) condition; derivation of eq 5; TS structure of the Volmer step on 1 ML/Pt and TS structures of the Tafel reaction on the 1 and 1.11 ML H/Pt(211). This material is available free of charge via the Internet at http://pubs.acs.org.

■ AUTHOR INFORMATION

Corresponding Author

*E-mail: zpliu@fudan.edu.cn.

Notes

The authors declare no competing financial interest.

■ ACKNOWLEDGMENTS

This work is supported by National Nature Science Foundation of China (20825311, 21173051, 21103110), 973 program (2011CB808500), Science and Technology Commission of Shanghai Municipality (08DZ2270500), Program for Professor of Special Appointment (Eastern Scholar), Innovation Program of Shanghai Municipal Education Commission (13YZ120), and China and Shanghai Postdoctoral Science Foundation (2012M520040, 12R21411200).

■ REFERENCES

(1) Solis, B. H.; Hammes-Schiffer, S. Substituent Effects on Cobalt Diglyoxime Catalysts for Hydrogen Evolution. *J. Am. Chem. Soc.* **2011**, *133*, 19036−19039.

(2) Li, Y. G.; Wang, H. L.; Xie, L. M.; Liang, Y. Y.; Hong, G. S.; Dai, H. J. MoS(2) Nanoparticles Grown on Graphene: An Advanced Catalyst for the Hydrogen Evolution Reaction. *J. Am. Chem. Soc.* **2011**, *133*, 7296−7299.

(3) Jiang, N.; Meng, H. M.; Song, L. J.; Yu, H. Y. Study on Ni-Fe-C cathode for hydrogen evolution from seawater electrolysis. *Int. J. Hydrogen Energy* **2010**, *35*, 8056−8062.

(4) Greeley, J.; Jaramillo, T. F.; Bonde, J.; Chorkendorff, I. B.; Norskov, J. K. Computational high-throughput screening of electrocatalytic materials for hydrogen evolution. *Nat. Mater.* **2006**, *5*, 909−913.

(5) Quaino, P.; Santos, E.; Wolfschmidt, H.; Montero, M. A.; Stimming, U. Theory meets experiment: Electrocatalysis of hydrogen oxidation/evolution at Pd-Au nanostructures. *Catal. Today* **2011**, *177*, 55−63.

(6) McCrory, C. C. L.; Uyeda, C.; Peters, J. C. Electrocatalytic Hydrogen Evolution in Acidic Water with Molecular Cobalt Tetraazamacrocycles. *J. Am. Chem. Soc.* **2012**, *134*, 3164−3170.

(7) Tavares, M. C.; Machado, S. A. S.; Mazo, L. H. Study of hydrogen evolution reaction in acid medium on Pt micro electrodes. *Electrochim. Acta* **2001**, *46*, 4359−4369.

(8) Seto, K. I., A.; Love, B.; Lipkowski, J. *J. Electroanal. Chem.* **1987**, *226*, 351.

(9) Gomez, R.; Fernandez-Vega, A.; Feliu, J.; Aldaz, A. Hydrogen evolution on platinum single crystal surfaces: effects of irreversibly adsorbed bismuth and antimony on hydrogen adsorption and evolution on platinum (100). *J. Phys. Chem.* **1993**, *97*, 4769−4776.

(10) Markovic, N. M.; Sarraf, S. T.; Gasteiger, H. A.; Ross, P. N. Hydrogen electrochemistry on platinum low-index single-crystal surfaces in alkaline solution. *J. Chem. Soc., Faraday Trans.* **1996**, *92*, 3719−3725.

(11) Markovic, N. M.; Grgur, B. N.; Ross, P. N. Temperature-dependent hydrogen electrochemistry on platinum low-index single-crystal surfaces in acid solutions. *J. Phys. Chem. B* **1997**, *101*, 5405−5413.

(12) Schmidt, T. J.; Ross, P. N.; Markovic, N. M. Temperature dependent surface electrochemistry on Pt single crystals in alkaline electrolytes Part 2. The hydrogen evolution/oxidation reaction. *J. Electroanal. Chem.* **2002**, *524*, 252−260.

(13) Barber, J. H.; Conway, B. E. Structural specificity of the kinetics of the hydrogen evolution reaction on the low-index surfaces of Pt single-crystal electrodes in 0.5 M dm(−3) NaOH. *J. Electroanal. Chem.* **1999**, *461*, 80−89.

(14) Conway, B. E.; Barber, J.; Morin, S. Comparative evaluation of surface structure specificity of kinetics of UPD and OPD of H at single-crystal Pt electrodes. *Electrochim. Acta* **1998**, *44*, 1109−1125.

(15) Conway, B. E.; Tilak, B. V. Interfacial processes involving electrocatalytic evolution and oxidation of H-2, and the role of chemisorbed H. *Electrochim. Acta* **2002**, *47*, 3571−3594.

(16) Hoshi, N.; Asaumi, Y.; Nakamura, M.; Mikita, K.; Kajiwara, R. Structural Effects on the Hydrogen Oxidation Reaction on n(111)-(111) Surfaces of Platinum. *J. Phys. Chem. C* **2009**, *113*, 16843−16846.

(17) Kajiwara, R.; Asaumi, Y.; Nakamura, M.; Hoshi, N. Active sites for the hydrogen oxidation and the hydrogen evolution reactions on the high index planes of Pt. *J. Electroanal. Chem.* **2011**, *657*, 61−65.

(18) Nakamura, M.; Kobayashi, T.; Hoshi, N. Structural dependence of intermediate species for the hydrogen evolution reaction on single crystal electrodes of Pt. *Surf. Sci.* **2011**, *605*, 1462−1465.

(19) Antoine, O.; Bultel, Y.; Durand, R.; Ozil, P. Electrocatalysis, diffusion and ohmic drop in PEMFC: Particle size and spatial discrete distribution effects. *Electrochim. Acta* **1998**, *43*, 3681−3691.

(20) Rao, C. V.; Viswanathan, B. Monodispersed Platinum Nanoparticle Supported Carbon Electrodes for Hydrogen Oxidation and Oxygen Reduction in Proton Exchange Membrane Fuel Cells. *J. Phys. Chem. C* **2010**, *114*, 8661−8667.

(21) Babic, B. M.; Vracar, L. M.; Radmilovic, V.; Krstajic, N. V. Carbon cryogel as support of platinum nano-sized electrocatalyst for the hydrogen oxidation reaction. *Electrochim. Acta* **2006**, *51*, 3820−3826.
(22) Bard, A. J.; Faulkner, L. R. *ELECTROCHEMICAL METHODS Fundamentals and Applications*, 2nd ed.; John Wiely & Sons Inc.: New York, NY, 2001.
(23) Wang, J. X.; Springer, T. E.; Adzic, R. R. Dual-pathway kinetic equation for the hydrogen oxidation reaction on Pt electrodes. *J. Electrochem. Soc.* **2006**, *153*, A1732−A1740.
(24) Strmcnik, D.; Tripkovic, D.; van der Vliet, D.; Stamenkovic, V.; Markovic, N. M. Adsorption of hydrogen on Pt(111) and Pt(100) surfaces and its role in the HOR. *Electrochem. Commun.* **2008**, *10*, 1602−1605.
(25) Skulason, E.; Tripkovie, V.; Bjorketun, M. E.; Gudmundsdottir, S.; Karlberg, G.; Rossmeisl, J.; Bligaard, T.; Jonsson, H.; Norskov, J. K. Modeling the Electrochemical Hydrogen Oxidation and Evolution Reactions on the Basis of Density Functional Theory Calculations. *J. Phys. Chem. C* **2010**, *114*, 18182−18197.
(26) Yang, F.; Zhang, Q. F.; Liu, Y. W.; Chen, S. L. A Theoretical Consideration on the Surface Structure and Nanoparticle Size Effects of Pt in Hydrogen Electrocatalysis. *J. Phys. Chem. C* **2011**, *115*, 19311−19319.
(27) Bjorketun, M. E.; Bondarenko, A. S.; Abrams, B. L.; Chorkendorff, I.; Rossmeisl, J. Screening of electrocatalytic materials for hydrogen evolution. *Phys. Chem. Chem. Phys.* **2010**, *12*, 10536−10541.
(28) Hamada, I.; Morikawa, Y. Density-functional analysis of hydrogen on Pt(111): Electric field, solvent, and coverage effects. *J. Phys. Chem. C* **2008**, *112*, 10889−10898.
(29) Cai, Y.; Anderson, A. B.; Angus, J. C.; Kostadinov, L. N. Hydrogen evolution on diamond electrodes by the volmer-Heyrovsky mechanism. *J. Electrochem. Soc.* **2007**, *154*, F36−F43.
(30) Ishikawa, Y.; Mateo, J. J.; Tryk, D. A.; Cabrera, C. R. Direct molecular dynamics and density-functional theoretical study of the electrochemical hydrogen oxidation reaction and underpotential deposition of H on Pt(111). *J. Electroanal. Chem.* **2007**, *607*, 37−46.
(31) Santana, J. A.; Mateo, J. J.; Ishikawa, Y. Electrochemical Hydrogen Oxidation on Pt(110): A Combined Direct Molecular Dynamics/Density Functional Theory Study. *J. Phys. Chem. C* **2010**, *114*, 4995−5002.
(32) Santos, E.; Hindelang, P.; Quaino, P.; Schmickler, W. A model for the Heyrovsky reaction as the second step in hydrogen evolution. *Phys. Chem. Chem. Phys.* **2011**, *13*, 6961−6969.
(33) Bhardwaj, M.; Balasubramaniam, R. A new method for determining kinetic parameters by simultaneously considering all the independent conditions at an overpotential in case of hydrogen evolution reaction following Volmer-Heyrovsky-Tafel mechanism. *Int. J. Hydrogen Energy* **2008**, *33*, 248−251.
(34) Skulason, E.; Karlberg, G. S.; Rossmeisl, J.; Bligaard, T.; Greeley, J.; Jonsson, H.; Norskov, J. K. Density functional theory calculations for the hydrogen evolution reaction in an electrochemical double layer on the Pt(111) electrode. *Phys. Chem. Chem. Phys.* **2007**, *9*, 3241−3250.
(35) Fang, Y. H.; Liu, Z. P. Mechanism and Tafel Lines of Electro-Oxidation of Water to Oxygen on RuO2(110). *J. Am. Chem. Soc.* **2010**, *132*, 18214−18222.
(36) Li, Y. F.; Liu, Z. P.; Liu, L. L.; Gao, W. G. Mechanism and Activity of Photocatalytic Oxygen Evolution on Titania Anatase in Aqueous Surroundings. *J. Am. Chem. Soc.* **2010**, *132*, 13008−13015.
(37) Wang, H. F.; Liu, Z. P. Formic Acid Oxidation at Pt/H_2O Interface from Periodic DFT Calculations Integrated with a Continuum Solvation Model. *J. Phys. Chem. C* **2009**, *113*, 17502−17508.
(38) Soler, J. M.; Artacho, E.; Gale, J. D.; Garcia, A.; Junquera, J.; Ordejon, P.; Sanchez-Portal, D. The SIESTA method for ab initio order-N materials simulation. *J. Phys.: Condens. Matter* **2002**, *14*, 2745−2779.
(39) Junquera, J.; Paz, O.; Sanchez-Portal, D.; Artacho, E. Numerical atomic orbitals for linear-scaling calculations. *Phys. Rev. B* **2001**, *64*, 235111.
(40) Troullier, N.; Martins, J. L. Efficient Pseudopotentials for Plane-Wave Calculations. *Phys. Rev. B* **1991**, *43*, 1993−2006.
(41) Perdew, J. P.; Burke, K.; Ernzerhof, M. Generalized gradient approximation made simple. *Phys. Rev. Lett.* **1996**, *77*, 3865−3868.
(42) Wang, H. F.; Liu, Z. P. Comprehensive mechanism and structure-sensitivity of ethanol oxidation on platinum: New transition-state searching method for resolving the complex reaction network. *J. Am. Chem. Soc.* **2008**, *130*, 10996−11004.
(43) Shang, C.; Liu, Z. P. Constrained Broyden Dimer Method with Bias Potential for Exploring Potential Energy Surface of Multistep Reaction Process. *J. Chem. Theory Comput.* **2012**, *8*, 2215.
(44) Shang, C.; Liu, Z. P. Constrained Broyden Minimization Combined with the Dimer Method for Locating Transition State of Complex Reactions. *J. Chem. Theory Comput.* **2010**, *6*, 1136−1144.
(45) Fang, Y. H.; Liu, Z. P. Toward Anticorrosion Electrodes: Site-Selectivity and Self-Acceleration in the Electrochemical Corrosion of Platinum. *J. Phys. Chem. C* **2010**, *114*, 4057−4062.
(46) Fang, Y. H.; Wei, G. F.; Liu, Z. P. Theoretical modeling of electrode/electrolyte interface from first-principles periodic continuum solvation method. *Catal. Today* **2013**, *202*, 98−104.
(47) Shang, C.; Liu, Z. P. Origin and Activity of Gold Nanoparticles as Aerobic Oxidation Catalysts in Aqueous Solution. *J. Am. Chem. Soc.* **2011**, *133*, 9938−9947.
(48) Wei, G. F.; Fang, Y. H.; Liu, Z. P. First Principles Tafel Kinetics for Resolving Key Parameters in Optimizing Oxygen Electrocatalytic Reduction Catalyst. *J. Phys. Chem. C* **2012**, *116*, 12696−12705.
(49) Fang, Y. H.; Liu, Z. P. Surface Phase Diagram and Oxygen Coupling Kinetics on Flat and Stepped Pt Surfaces under Electrochemical Potentials. *J. Phys. Chem. C* **2009**, *113*, 9765−9772.
(50) Hitotsuyanagi, A.; Nakamura, M.; Hoshi, N. Structural effects on the activity for the oxygen reduction reaction on n(111)-(100) series of Pt: correlation with the oxide film formation. *Electrochim. Acta* **2012**, *82*, 512−516.
(51) Karlberg, G. S.; Jaramillo, T. F.; Skulason, E.; Rossmeisl, J.; Bligaard, T.; Norskov, J. K. Cyclic voltammograms for H on Pt(111) and Pt(100) from first principles. *Phys. Rev. Lett.* **2007**, *99*, 126101.
(52) Santos, E.; Hindelang, P.; Quaino, P.; Schulz, E. N.; Soldano, G.; Schmickler, W. Hydrogen Electrocatalysis on Single Crystals and on Nanostructured Electrodes. *ChemPhysChem* **2011**, *12*, 2274−2279.
(53) Markovic, N.; Ross, P., Jr. Surface science studies of model fuel cell electrocatalysts. *Surf. Sci. Rep.* **2002**, *45*, 117−229.
(54) Kunimatsu, K.; Uchida, H.; Osawa, M.; Watanabe, M. In situ infrared spectroscopic and electrochemical study of hydrogen electro-oxidation on Pt electrode in sulfuric acid. *J. Electroanal. Chem.* **2006**, *587*, 299−307.
(55) Kunimatsu, K.; Senzaki, T.; Samjeske, G.; Tsushima, M.; Osawa, M. Hydrogen adsorption and hydrogen evolution reaction on a polycrystalline Pt electrode studied by surface-enhanced infrared absorption spectroscopy. *Electrochim. Acta* **2007**, *52*, 5715−5724.
(56) Chun, J.; Ra, K.; Kim, N. The Langmuir adsorption isotherms of electroadsorbed hydrogens for the cathodic hydrogen evolution reactions at the Pt $(100)/H_2SO_4$ and LiOH aqueous electrolyte interfaces. *Int. J. Hydrogen Energy* **2001**, *26*, 941−948.
(57) *CRC Handbook of Chemistry and Physics*, 84th ed.; Lide, D. R., Ed.; CRC Press: Boca Raton, FL, 2003−2004.
(58) Liu, Z. P.; Hu, P. General trends in CO dissociation on transition metal surfaces. *J. Chem. Phys.* **2001**, *114*, 8244−8247.
(59) Liu, Z. P.; Hu, P.; Alavi, A. Catalytic role of gold in gold-based catalysts: A density functional theory study on the CO oxidation on gold. *J. Am. Chem. Soc.* **2002**, *124*, 14770−14779.
(60) Parsons, R. The rate of electrolytic hydrogen evolution and the heat of adsorption of hydrogen. *Trans. Faraday. Soc.* **1958**, *54*, 1053−1063.
(61) Norskov, J. K.; Bligaard, T.; Logadottir, A.; Kitchin, J. R.; Chen, J. G.; Pandelov, S. Trends in the exchange current for hydrogen evolution. *J. Electrochem. Soc.* **2005**, *152*, J23−J26.

(62) Sun, Y.; Dai, Y.; Liu, Y. W.; Chen, S. L. A rotating disk electrode study of the particle size effects of Pt for the hydrogen oxidation reaction. *Phys. Chem. Chem. Phys.* **2012**, *14*, 2278−2285.